Interaction of intense vuv radiation with large xenon clusters

Zachary B. Walters,[1] Robin Santra,[2] and Chris H. Greene[1]

[1]*Department of Physics and JILA, University of Colorado, Boulder, Colorado 80309-0440, USA*
[2]*Argonne National Laboratory, Argonne, Illinois 60439, USA*
(Received 19 April 2006; published 26 October 2006)

The interaction of atomic clusters with short, intense pulses of laser light to form extremely hot, dense plasmas has attracted extensive experimental and theoretical interest. The high density of atoms within the cluster greatly enhances the atom-laser interaction, while the finite size of the cluster prevents energy from escaping the interaction region. Recent technological advances have allowed experiments to probe the laser-cluster interaction at very high photon energies, with interactions much stronger than suggested by theories for lower photon energies. We present a model of the laser-cluster interaction that uses nonperturbative *R*-matrix techniques to calculate inverse bremsstrahlung and photoionization cross sections for Herman-Skillman atomic potentials. We describe the evolution of the cluster under the influence of the processes of inverse bremsstrahlung heating, photoionization, collisional ionization and recombination, and expansion of the cluster. We compare total energy absorbed with the Hamburg experiment of Wabnitz *et al.* [Nature **420**, 482 (2002)] and ejected electron spectra with Laarmann *et al.* [Phys. Rev. Lett. **95**, 063402 (2005)].

I. INTRODUCTION

At sufficiently low temperatures and sufficiently high density, atoms and molecules in the gas phase begin to form bound systems, or clusters [1,2]. Some clusters consist of only a few monomers; others contain many millions of atoms or molecules. In this sense, clusters, which are typical nano-materials, represent a natural link between simple atoms and condensed matter. However, they do not simply mimic the properties of their constituents nor of the bulk to which they converge. Clusters are unique. This is highlighted, for example, by their interaction with intense electromagnetic radiation.

The majority of corresponding experiments were carried out using laser pulses in the near-infrared, with photon energies of about 1 eV and pulse durations on the order of 100 fs [3]. At pulse intensities of 10^{16} W/cm^2 or higher, noble gas clusters consisting of krypton or argon atoms absorb the laser pulse energy extremely efficiently. They are turned into nanoplasmas accompanied by high ionic charge states and strong x-ray emission [4]. In xenon clusters, the production of extremely hot (keV) electrons was observed [5]. The hot nanoplasmas undergo complete fragmentation. Experimental studies of the associated dynamics have been carried out for Ar and Xe clusters by Lezius *et al.* [6]: ions with kinetic energies of up to 1 MeV are found to be ejected from the expanding clusters.

The high density of atoms in the cluster greatly enhances the atom-laser interaction over that of lone atoms, while the finite size of the clusters ensures that energy absorbed by the cluster is largely constrained to stay within the interaction region, not carried off by a large heat bath, as occurs with materials in bulk. These properties in combination allow the laser-cluster interaction to create extremely hot, dense plasmas, which may in turn serve as sources for high-energy particles or photons.

Several groups performed extensive numerical simulations with the purpose of identifying the relevant heating mechanisms. Ditmire *et al.* [7] pointed out that collisional heating dominates. More precisely, the ionized electrons inside the cluster are quasifree but can absorb photons whenever they are being scattered by ions. This process is referred to as *inverse bremsstrahlung* [8]. Inelastic electron-ion collisions of the $(e, 2e)$-type contribute to the high ionic charge states observed. Other authors [9–11] concentrated on the interplay between the strong quasistatic electric field of the laser and the Coulomb field of neighboring ions. This interplay can lead to *enhanced ionization*, first discovered in diatomic molecules [12,13]. The relative importance of enhanced ionization is somewhat difficult to assess, since in Refs. [9–11] collisional heating was not considered and no comparison was provided between the simulations and available experimental data.

Little is known about laser-cluster interactions at uv or higher photon energies. The destructive impact of laser pulses with a peak intensity of almost 10^{19} W/cm^2 at a wavelength of 248 nm was demonstrated by McPherson *et al.* [14]. However, intense laser fields at even higher photon energies have not been accessible until very recently. In 2000, the first lasing—in a free-electron laser (FEL)—at $\lambda = 109$ nm was reported [15]. The FEL is part of the TESLA Test Facility (TTF) in Hamburg, Germany. (One of the major objectives of the TTF is the development of the technology for an ultrabright x-ray laser.) The new vuv laser source has already displayed its capability for exploring interesting physics: Motivated by the outstanding properties of the radiation generated by the TTF FEL, documented in Ref. [16], experiments were performed [17] in which Van der Waals clusters of xenon atoms were exposed to 12.7-eV vuv photons, an energy range that had been previously unexplored.

Each pulse in the experiment lasted about 100 fs. The highest intensity in the experiment was about 7×10^{13} W/cm^2. Under these conditions, isolated Xe atoms were found to produce only singly charged ions (see Refs. [18,19] for recent developments). In large clusters, however, each atom was found to absorb up to 400 eV, corresponding

to 30 photons, and charge states of up to 8 plus were detected.

These results were very surprising. The dominant processes in most models of infrared laser-cluster interactions are field ionization of atoms by the strong electric field of the laser, and heating of the cluster through inelastic dephasing collisions by electrons oscillating in the laser electric field. Both of these processes are strongly inhibited by the high frequency of the vuv photons. A relevant quantity in this context is the ponderomotive potential [20] of an electron oscillating in a laser field. At a laser intensity of 7 $\times 10^{13}$ W/cm^2, the ponderomotive potential is only 62 meV, which is smaller than the ionization potential of atomic xenon (12.1 eV [21]) by three orders of magnitude.

In a previous Letter, two of us [22] proposed that the additional heating was due to the effects of atomic structure on the inverse bremsstrahlung rates. However, that initial study calculated the inverse bremsstrahlung rates using perturbation theory for both the electron-photon interaction and the electron-ion interaction. The method implemented for this paper instead treats the electron-ion interaction nonperturbatively using variational R-matrix methods, while retaining first-order perturbation theory for the electron-photon interaction. The resulting photoionization and inverse bremsstrahlung cross sections calculated are expected to be more realistic, even though our description remains at the independent electron level.

In this paper, we present a model of the laser-cluster interaction that takes atomic structure and the effects of plasma screening into account more fully than previous approaches to the subject. Considering the limitations of the model and the poor experimental characterization of the FEL radiation [23], we achieve good agreement with the Hamburg results. We track photoionization, collisional ionization and recombination, inverse bremsstrahlung heating, evaporation of electrons from the cluster, and expansion of the cluster due to hydrodynamic pressure of hot electrons and Coulomb repulsion through the duration of the laser pulse and, later, as the cluster undergoes a Coulomb explosion.

Atomic units are used throughout, unless otherwise noted.

II. PHOTOIONIZATION

A novel feature of the Hamburg experiment is that the 12.7-eV photons are sufficient to overcome the 12.1-eV ionization potential of neutral xenon. Therefore, although the oscillating electric field is too weak for the xenon atoms to undergo field ionization, as occurs in the infrared domain, there is still an efficient optical process for creating Xe$^+$. Friedrich [24] gives the cross section for the transition from the bound state $|\phi_i\rangle$ to the continuum state $|\phi_f\rangle$ as

$$\sigma_{fi}(E) = 4\pi^2 \alpha \omega |\vec{\pi} \cdot \vec{r}_{fi}|^2, \tag{1}$$

where α is the fine-structure constant, ω is the photon energy, $\vec{\pi}$ is the polarization vector for the radiation, and $\vec{r}_{fi} = \langle \phi_f | \vec{r} | \phi_i \rangle$ is the dipole matrix element coupling the initial and final states of the electron. The wave function of the photoelectron in Eq. (1) is energy-normalized. E stands for the kinetic energy of the photoelectron.

For linearly polarized light, chosen without loss of generality to be polarized in the $\hat{z}$ direction, the matrix element that must be found is

$$\langle \phi_f | z | \phi_i \rangle = I_R(l_i, l_f) \int d\Omega Y^*_{l_f m_f}(\Omega) \cos(\theta) Y_{l_i m_i}(\Omega). \tag{2}$$

Here,

$$I_R(l_i, l_f) = \int_0^\infty dr U_f(r) r U_i(r), \tag{3}$$

where $U(r) = r R(r)$ denotes the rescaled radial wave function. Equations (1) and (2) refer to specific angular momentum quantum numbers l and m for the initial and final states. At a photon energy of 12.7 eV, only the $5p$ electrons of xenon can respond to the radiation field. Hence, we can focus on a subshell with fixed l_i (here, $l_i = 1$). Let q stand for the number of electrons in this subshell. Then, within the independent particle model, after averaging over the initial and summing over the final one-electron states, the total atomic photoionization cross section is given by

$$\sigma_{PI} = q \frac{4}{3} \pi^2 \frac{\alpha \omega}{2l_i + 1} \times \{l_i I_R^2(l_i, l_i - 1) + (l_i + 1) I_R^2(l_i, l_i + 1)\}. \tag{4}$$

The identities [25,26]

$$\int d\Omega Y^*_{l_1 m_1}(\Omega) \cos(\theta) Y_{l_2 m_2}(\Omega) = \sqrt{(2l_1 + 1)(2l_2 + 1)}$$

$$\times (-1)^{-m_1} \begin{pmatrix} l_1 & 1 & l_2 \\ -m_1 & 0 & m_2 \end{pmatrix}$$

$$\times \begin{pmatrix} l_1 & 1 & l_2 \\ 0 & 0 & 0 \end{pmatrix}, \tag{5}$$

$$\sum_{m_1, m_2} \begin{pmatrix} l_1 & l_2 & l_3 \\ m_1 & m_2 & m_3 \end{pmatrix} \begin{pmatrix} l_1 & l_2 & l_3' \\ m_1 & m_2 & m_3' \end{pmatrix} = \frac{\delta(l_3, l_3') \delta(m_3, m_3')}{2l_3 + 1}, \tag{6}$$

and

$$(2l_1 + 1)(2l_2 + 1) \begin{pmatrix} l_1 & 1 & l_2 \\ 0 & 0 & 0 \end{pmatrix}^2 = \begin{cases} l_1 + 1 & \text{if } l_2 = l_1 + 1 \\ l_1 & \text{if } l_2 = l_1 - 1 \\ 0 & \text{otherwise} \end{cases} \tag{7}$$

have been exploited in the derivation of Eq. (4). $\begin{pmatrix} l_1 & l_2 & l_3 \\ m_1 & m_2 & m_3 \end{pmatrix}$ represents the Wigner 3-j symbol, related to the Clebsch-Gordan coefficient by

$$\begin{pmatrix} l_1 & l_2 & l \\ m_1 & m_2 & m \end{pmatrix} = \frac{(-1)^{l_1 - l_2 - m}}{\sqrt{2l + 1}} \times \langle l_1 m_1 l_2 m_2 | l_1 l_2 l - m \rangle. \tag{8}$$

The radial integrals $I_R(l_i, l_f)$ [Eq. (3)] were calculated in the acceleration representation, using wave functions generated in a variational eigenchannel R-matrix calculation [27], using a B-spline basis set to describe electrons that experi-

ence a Hartree-Slater atomic potential. This potential, which was calculated employing the program by Herman and Skill-man [28], is spherically symmetric. Its eigenstates may therefore be chosen as eigenstates of orbital angular momentum.

As a consequence of efficient photoionization, the electrons and ions inside the cluster form a dense, nanoscale-sized plasma already at an early stage of the laser pulse. This plasma has the effect of screening the atomic potential from both bound and continuum electrons. This lowers the ionization potential and changes both the initial- and final-state electron wave functions. Because of this, cross sections for photoionization become larger as the screening length in the plasma becomes shorter. With sufficient screening, it becomes possible for ions to undergo additional photoionization.

To account for this process, the screened radial matrix elements were calculated using the same R-matrix methods as for isolated Xe atoms. However, before the initial- and final-state wave functions were calculated, the Herman-Skillman potential was multiplied by a Debye screening factor $\exp(-r/\lambda_D)$. [The electron Debye length is defined as $\lambda_D = \sqrt{T/(4\pi n_e)}$ [29]. The electron temperature T in this expression is measured in units of energy. n_e is the electron density.] Both the matrix elements and the corresponding photoionization potentials were then spline-interpolated in the process of calculating the photoionization cross section at a given screening length. For most of this paper, this screening length was restricted to be no less than the Wigner-Seitz radius of xenon at liquid density, 4.64 bohr. A discussion of shorter screening lengths is given in a later section.

III. INVERSE BREMSSTRAHLUNG HEATING

A second effect of having a high density of free electrons in the cluster plasma is that these electrons can themselves undergo both stimulated and inverse bremsstrahlung, creating a second mechanism through which laser energy can be deposited into the cluster. Stimulated (inverse) bremsstrahlung refers to photon emission into (absorption from) the laser mode by an electron colliding with an ion in the plasma.

We treat the collisions of an electron with the cluster ions as independent events in both time and space. This allows us to focus on a single collision of an electron with a single ion embedded in the plasma. The cross section per unit energy for a free-free transition from initial state $|\phi_{E',l',m'}\rangle$ to final state $|\phi_{E,l,m}\rangle$ can be shown, using Fermi's golden rule, to equal

$$\sigma_{E,l,m \leftarrow E',l',m'} = \frac{4\pi^2\alpha}{\omega^3}\left|\langle\phi_{E,l,m}|\frac{\partial V}{\partial z}|\phi_{E',l',m'}\rangle\right|^2. \quad (9)$$

In the case of photon emission (absorption), $E=E'-\omega$ ($E=E'+\omega$). Equation (9) describes the interaction of linearly polarized radiation in the acceleration representation. V is the plasma-screened atomic potential experienced by the scattered electron.

As with photoionization cross sections, radial wave functions were calculated using a nonperturbative eigenchannel

R-matrix approach. Matrix elements between the energy-normalized wave functions were then calculated in the acceleration gauge, where the $1/r^2$ long-range dependence of $\partial V/\partial z$ ensures that the radial integral will converge, although the continuum electron wave functions are not spatially normalizable.

Although microscopic reversibility ensures that absorption and emission cross sections coincide, stimulated free-free transitions act as a powerful heating process because lower-energy states are more highly populated than higher-energy states in a thermal distribution. Heating rates can then be calculated for any given electron distribution. In this study, we assume that after each photon absorption or emission event the electron gas reequilibrates rapidly as a consequence of frequent electron-electron collisions. Thus, the electron probability distribution $\rho(E)$ may be written at all times during the laser pulse as a Maxwell-Boltzmann distribution,

$$\rho(E) = 2\sqrt{\frac{E}{\pi T^3}}e^{-E/T}. \quad (10)$$

The cross section defined in Eq. (9) describes a free-free transition between orbital angular momentum eigenstates. We therefore introduce $\rho(E,l,m)$, which is the probability per unit energy to find an electron in the state $|\phi_{E,l,m}\rangle$. Clearly, $\rho(E)=\Sigma_{l,m}\rho(E,l,m)$. If the wave function is normalized within a large sphere of radius R (not to be confused with the cluster radius), then the largest l that contributes to this sum at a given kinetic energy E is $l_{max}=R\sqrt{2E}$ [30]. Since, in thermal equilibrium, $\rho(E,l,m)$ can depend only on E, we see that

$$\rho(E,l,m) = \frac{\rho(E)}{2R^2E} \quad (11)$$

in the limit of large R ($l_{max} \gg 1$).

We are interested in radiation-induced heating, i.e., in the change of the electron temperature due to photon absorption and emission. To this end, we will derive from

$$\frac{\partial T}{\partial t} = \frac{2}{3}\int_0^\infty dE\,E\sum_{l,m}\frac{\partial\rho(E,l,m)}{\partial t} \quad (12)$$

a rate equation for the electron temperature, expressed in terms of the cross sections for stimulated and inverse bremsstrahlung [Eq. (9)]. When writing down the equation for the time evolution of $\rho(E,l,m)$, we must take into consideration that $\rho(E,l,m)$ refers to (spherical) box normalization, while the cross section per unit energy in Eq. (9) is based on energy-normalized wave functions. For the sake of consistency, it is necessary to change the initial state in the free-free radiative transition in Eq. (9) from energy normalization to box normalization. This has the effect of multiplying the cross section by $\pi\sqrt{2E}/R$.

Hence, in the presence of N_a atomic scatterers (within the normalization volume) and a laser beam of intensity I, the rate of change of $\rho(E,l,m)$ is given by

$$\frac{\partial \rho(E,l,m)}{\partial t} = N_a \frac{I}{\omega} \frac{\sqrt{2}\pi}{R}$$

$$\times \sum_{l',m'} \{ \sigma_{E,l,m\leftarrow E-\omega,l',m'} \sqrt{E-\omega}\,\rho(E-\omega,l',m')$$

$$+ \sigma_{E,l,m\leftarrow E+\omega,l',m'} \sqrt{E+\omega}\,\rho(E+\omega,l',m')$$

$$- \sigma_{E+\omega,l',m'\leftarrow E,l,m} \sqrt{E}\,\rho(E,l,m)$$

$$- \sigma_{E-\omega,l',m'\leftarrow E,l,m} \sqrt{E}\,\rho(E,l,m) \}. \tag{13}$$

The first two terms in the curly brackets in Eq. (13) describes the population of $|\phi_{E,l,m}\rangle$ via photoabsorption (photoemission) from states with energy $E-\omega$ ($E+\omega$); the second two terms describe the depopulation of $|\phi_{E,l,m}\rangle$ due to photoabsorption and photoemission from this state. Equation (13) implies a nondegenerate electron gas.

An electron state with energy E, then, communicates with states of energy $E-\omega$, which are on average more densely populated than itself. Since the absorption and emission cross sections are equal, this tends to populate the state of energy E and depopulate the states of energy $E-\omega$, resulting in a net heating process. The state will also communicate with states of energy $E+\omega$, which are less densely populated than itself, thereby again tending to populate the higher-energy states while depopulating the lower-energy state.

Combining Eqs. (10)–(13), we are led in a natural way to the following definition of the inverse bremsstrahlung cross section (per unit energy):

$$\sigma_{E+\omega\leftarrow E} = \sum_{l,m} \sum_{l',m'} \sigma_{E+\omega,l,m\leftarrow E,l',m'}. \tag{14}$$

Using Eqs. (5)–(7) and (9), this can be written as

$$\sigma_{E+\omega\leftarrow E} = \frac{4}{3}\pi^2 \frac{\alpha}{\omega^3} \times \sum_l \{l J_R^2(l,l-1) + (l+1)J_R^2(l,l+1)\}, \tag{15}$$

where

$$J_R(l,l') = \int_0^\infty dr\, U_{E+\omega,l}(r) \frac{dV}{dr} U_{E,l'}(r). \tag{16}$$

The rate of change of the electron temperature due to inverse bremsstrahlung is then

$$\frac{\partial T}{\partial t} = \frac{2}{9} n_a I \left(\frac{2\pi}{T}\right)^{3/2} [1 - e^{-\omega/T}] \times \int_0^\infty dE\, e^{-E/T} \sigma_{E+\omega\leftarrow E}. \tag{17}$$

The parameter n_a stands for the number of atoms per unit volume. In general, the ions in the plasma are not all in the same charge state. Denoting the fraction of Xe^{i+} by $f^{(i)}$, $\sigma_{E+\omega\leftarrow E}$ in Eq. (17) is replaced with $\Sigma_i f^{(i)} \sigma^{(i)}_{E+\omega\leftarrow E}$, where $\sigma^{(i)}_{E+\omega\leftarrow E}$ is the inverse bremsstrahlung cross section in the field of Xe^{i+}.

Figures 1 and 2 illustrate the dramatic effects of the ionic potential on the inverse bremsstrahlung cross section. In Fig. 1, as the scattering electron collides with the ion at higher
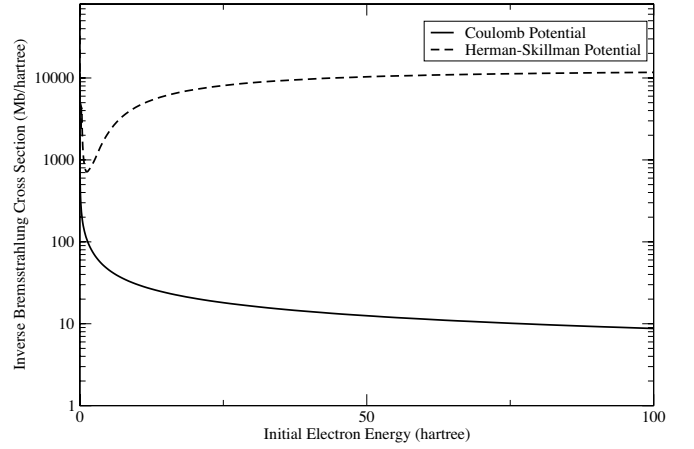

FIG. 1. Inverse bremsstrahlung cross sections [Eqs. (14) and (15)] for an electron with incident energy E to absorb a 12.7-eV photon are given for an electron in the field of a purely Coulombic 1+ potential and for an electron in the field of a Xe Herman-Skillman atomic potential. The effects of atomic structure on inverse bremsstrahlung rates are quite pronounced.

and higher initial energies, it probes regions of the ionic potential at which the ion nucleus is screened increasingly poorly by inner-shell electrons. As a result, the inverse bremsstrahlung cross section rises to many hundreds of times that of the naked Coulomb potential.

Adding plasma screening to this picture has the effect of supplementing the screening effects of inner-shell electrons with the screening effects of plasma electrons. As a result, the scattering electron feels the effects of the ionic nucleus more strongly than in the pure Coulomb case, but less strongly than in the case of the unscreened ionic potential. This is seen in a steady decrease of the inverse bremsstrahlung cross section as the screening range decreases.
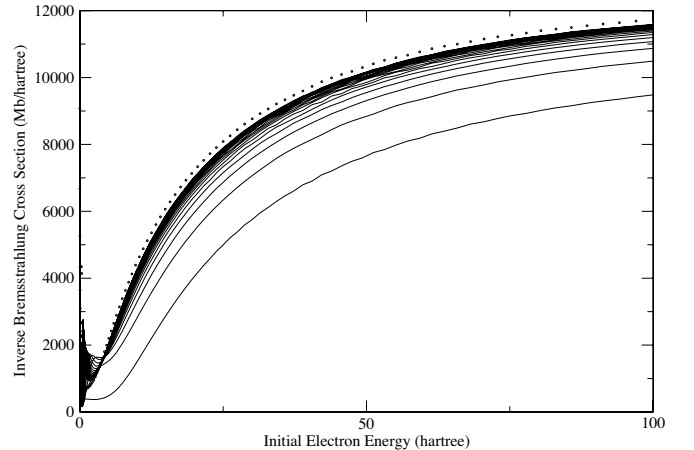

FIG. 2. The inverse bremsstrahlung cross section as a function of energy is shown for an electron in the field of a Debye-screened Xe Herman-Skillman potential, with the Debye screening length λ_D ranging from 1 to 20 a.u. As λ_D grows, the cross section approaches the limit of no plasma screening, shown in this graph by the dotted line. As the Debye length of the cluster plasma shrinks, the charged ion is shielded more effectively from the scattering electron, and the inverse bremsstrahlung cross section is decreased.

IV. COLLISIONAL IONIZATION AND RECOMBINATION

Although photoionization and inverse bremsstrahlung are the only processes by which the cluster can absorb photons from the laser beam, they are not by themselves sufficient to explain the cluster's evolution. As the pulse progresses, large numbers of free electrons fill the cluster. These electrons can liberate other electrons via collisional ionization if they have sufficient energy, or they can undergo three-body recombination with an ion.

Including the effects of ionization and recombination, the rate equation for the number per unit volume n_i of charge species i is given by

$$\frac{\partial n_i}{\partial t} = \frac{I}{\omega}(\sigma_{PI}^{i-1}n_{i-1} - \sigma_{PI}^{i}n_i) + S_{i-1}n_{i-1}n_e - S_in_in_e + R_{i+1}n_{i+1}n_e^2$$
$$- R_in_in_e^2, \tag{18}$$

where n_e is the number of electrons per unit volume. The photoionization cross sections σ_{PI}^j were calculated in Sec. II. The ionization and recombination coefficients S_i and R_i for the reaction $Xe^{i+} + e^- \rightarrow Xe^{(i+1)+} + 2e^-$ are calculated later in this section.

These rate equations, along with equations for the energy in the free-electron gas and the radius of the cluster, are integrated numerically through the duration of the pulse. As a general rule, this set of equations will be quite stiff. We performed this integration using the Rosenbrock method [31].

There are two requirements for a satisfactory treatment of collisional ionization and recombination in the cluster. First, both processes must occur at appropriate rates, and second, the rates for ionization and recombination must be consistent with one another, in that they drive the cluster toward chemical equilibrium at all times. The second requirement is particularly significant because the usual treatment of collisional ionization (also used in this study) uses the semiempirical Lotz formula [32] for ionization from the jth subshell,

$$S_i^j = 6.7 \times 10^{-7}\frac{a_jq_i^j}{T^{3/2}}\left(\frac{1}{P_j/T}\int_{P_j/T}^{\infty}\frac{e^{-x}}{x}dx\right.$$
$$\left. - \frac{b_j\exp(c_j)}{P_j/T + c_j}\int_{P_j/T+c_j}^{\infty}\frac{e^{-y}}{y}dy\right)\frac{cm^3}{s}, \tag{19}$$

to find ionization coefficients, where a_j, b_j, c_j are semiempirical constants, q_i^j is the number of equivalent electrons Xe^{i+} contains in the jth subshell, P_j is the ionization potential, and T is the temperature. For charge states of $0,\dots,5+$, we choose semiempirical constants corresponding to the $5p$ sublevel. For charge states of $6+$ and $7+$, which have no $5p$ electrons in the ground state, we choose constants corresponding to the $5s$ sublevel. Because this formula is only a semiempirical approximation, it is important to use recombination coefficients that are consistent with the ionization coefficients to prevent the model from settling into an incorrect equilibrium charge distribution.

The ratio between ionization and recombination coefficients can be obtained using the concept of equilibrium constants. In a plasma at equilibrium, the rate of collisions ionizing Xe^{i+} to form $Xe^{(i+1)+} + e^-$ must be equal to the rate at which $Xe^{(i+1)+} + e^-$ recombines to form Xe^{i+}. The recombination coefficients found in this manner can then be applied to modeling the cluster plasma, which is not, in general, in a state of chemical equilibrium.

These two rates are given, respectively, by

$$S_in_in_e = \text{rate of ionizing collisions} \tag{20}$$

and

$$R_{i+1}n_{i+1}n_e^2 = \text{rate of recombining collisions}. \tag{21}$$

Hence, the ratio S/R is given by

$$\frac{S_i}{R_{i+1}} = \frac{n_{i+1}^{eq}n_e^{eq}}{n_i^{eq}}. \tag{22}$$

The fraction $(n_{i+1}^{eq}n_e^{eq})/n_i^{eq}$ is known as the equilibrium constant for the reaction, and can be calculated thermodynamically.

In any reaction $A \rightarrow B + C$ at equilibrium, the chemical potentials for the forwards and backwards reactions must be balanced, $\mu_A = \mu_B + \mu_C$. The chemical potential of each species is given by a partial derivative of the Helmholtz free energy,

$$\mu_i = \frac{\partial F}{\partial N_i}T,V. \tag{23}$$

The Helmholtz free energy is given by $F = -T \ln Z_{tot}$, where Z_{tot} is the partition function for the system as a whole.

Factoring the total partition function into the product of individual particle partition functions (which implies independent particles),

$$Z_{tot}(N_A,N_B,N_C,V,T) = Z_A(N_A,V,T)Z_B(N_B,V,T)Z_C(N_C,V,T)$$
$$= \frac{z_A(V,T)^{N_A}}{N_A!}\frac{z_B(V,T)^{N_B}}{N_B!}\frac{z_C(V,T)^{N_C}}{N_C!}, \tag{24}$$

and assuming $N_i \gg 1$ yields

$$\mu_i = -T\frac{\partial \ln(Z_i(V,T))}{\partial N_i} = -T \ln\left(\frac{z_i}{N_i}\right). \tag{25}$$

Imposing balanced chemical potentials yields

$$\frac{N_BN_C}{N_A} = \frac{z_B(V,T)z_C(V,T)}{z_A(V,T)} \tag{26}$$

or equivalently

$$K_{eq}(T) = \frac{n_Bn_C}{n_A} = \frac{\dfrac{z_B(V,T)}{V}\dfrac{z_C(V,T)}{V}}{\dfrac{z_A(V,T)}{V}}, \tag{27}$$

where the equilibrium constant K_{eq} is a function of temperature only.

If the ionization potential of Xe^{i+} is given by P_i, then the partition functions are given by

$$z_i = \int_0^\infty dE e^{-E/T} \rho_i(E),$$

$$z_{i+1} = e^{-P_i/T} \int_0^\infty dE e^{-E/T} \rho_{i+1}(E),$$

$$z_e = \int_0^\infty dE e^{-E/T} \rho_e(E). \tag{28}$$

Through most of the lifetime of the pulse, tight plasma screening destroys the Rydberg states and most of the internal degrees of freedom of the various ions, leaving the density of states $\rho(E)$ dominated by the center-of-mass term and by a combinatorial term

$$D(i) = \binom{m}{n} \tag{29}$$

accounting for the number of ways n electrons can be distributed in m orbitals. For charge states up to 6+, we use $m=6$, $n=6-i$. For 7+ and 8+, we use $m=2$, $n=8-i$. If we exploit this by setting $\rho_i(E)/D(i) = \rho_{i+1}(E)/D(i+1)$, the common integral in z_i and z_{i+1} falls out of the equilibrium constant, yielding

$$K_{eq}^{(Xe^{i+} \to Xe^{(i+1)+}+e^-)} = e^{-P_i/T} \frac{T^{3/2} D(i+1)}{\sqrt{2}\pi^{3/2} D(i)}. \tag{30}$$

Equation (30) can now be combined with Eqs. (19) and (22) to yield recombination rate coefficients that have appropriate magnitude and that, in combination with the ionization coefficients, drive the system toward the correct equilibrium distribution at all times.

A gas of charged particles has different thermodynamic properties from an ideal gas due to Coulomb interactions between the constituent particles. Zel'dovich and Raizer [33] calculate the adjustment to K_{eq} due to a Debye-Hückel potential. The equilibrium constant including Coulomb effects can be written

$$K_{eq}^{(Xe^{i+} \to Xe^{(i+1)+}+e^-)} = e^{-(P_i+\Delta P_i)/T} \frac{T^{3/2} D(i+1)}{\sqrt{2}\pi^{3/2} D(i)}, \tag{31}$$

where the change in ionization potential due to Coulomb effects is $\Delta P_i = -(Q_i+1)/\lambda_D$, the Coulomb potential between the ion core and an electron held at distance λ_D.

In our approach, by explicitly calculating bound-state energies for Debye-screened Hartree-Slater potentials, we calculate this adjustment to the ionization potential directly. Our adjustment behaves similarly to the Zel'dovich and Raizer correction, but is larger for longer screening lengths and smaller at shorter screening lengths.

One advantage to the equilibrium constant approach is that conceptually it separates information about thermodynamic balance from the rate at which the system seeks that balance. As a result, any formula for ionization or recombination coefficients could be substituted for the Lotz formula,
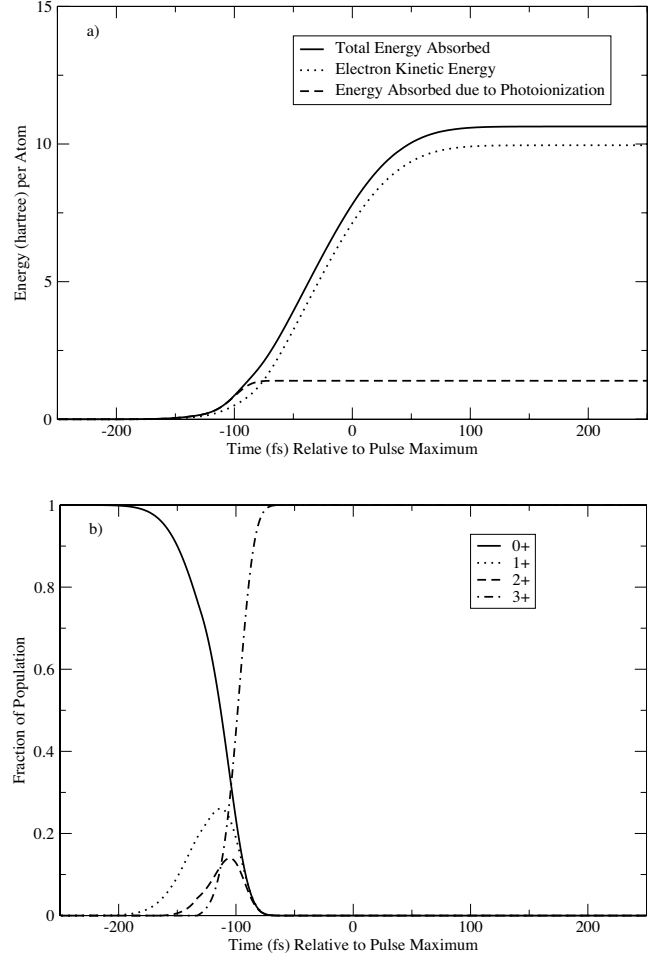

FIG. 3. Evolution of a 1500-atom cluster exposed to a 100 fs, 7×10^{13} W/cm^2 pulse, employing only photoionization and inverse bremsstrahlung heating. (a) Energy absorbed vs time. (b) Ionic population vs time. Xe^{2+} and Xe^{3+} are produced efficiently via photoionization.

with the accuracies of the overall rate and of the equilibrium constant used being the only criteria for the validity of the formula.

Including the effects of collisional ionization and recombination has a pronounced effect on the evolution of the cluster. In Fig. 3, the evolution of the cluster is calculated employing only photoionization and inverse bremsstrahlung. In contrast, Fig. 4 shows the evolution of the same cluster employing photoionization, inverse bremsstrahlung, collisional ionization and recombination, and evaporation of energetic electrons from the cluster. Allowing ionization and recombination has the effect of producing charge states up to Xe^{8+} in substantial quantities, and of nearly doubling the energy per atom absorbed by the cluster.

V. CLUSTER DYNAMICS DURING THE LASER PULSE

As the cluster absorbs energy from the laser field, some of the electrons become so energetic that they are no longer bound to the cluster. In addition, the cluster expands and cools due to hydrostatic forces from the hot electrons and
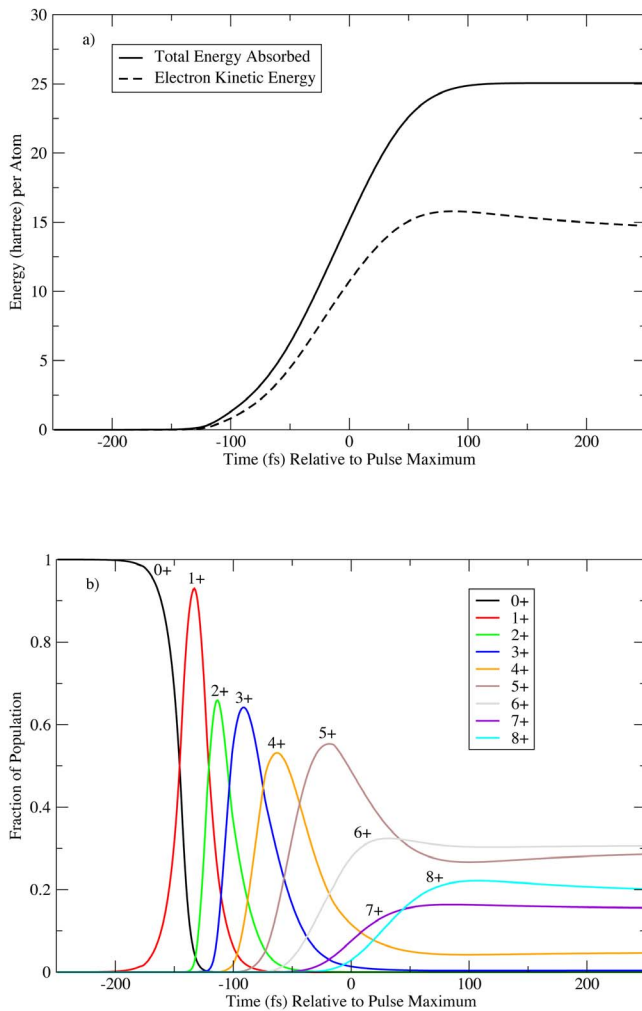
FIG. 4. (Color online) The effects of collisional ionization and recombination are to allow the formation of charge states beyond Xe^{3+}. Pictured is the time evolution of a single 1500-atom cluster exposed to a 100 fs, 7×10^{13} W/cm^2 pulse. These high charge states enhance the rate of inverse bremsstrahlung heating. As the plasma expands and cools, the chemical equilibrium shifts toward lower charge states on a time scale much longer than the laser pulse, until decreasing plasma density causes recombination and ionization rates to go to zero. (a) Energy absorbed vs time. (b) Ionic population vs time during laser pulse.

Coulomb repulsion as escaping electrons leave a charge imbalance behind. These in turn affect the microscopic processes inside the cluster, since all such processes depend on the concentrations of charge species within the cluster. Collisional ionization and recombination are also sensitively dependent on the temperature of the electron gas relative to electron binding energy.

We tested our assumption that the electron gas reequilibrates rapidly relative to the rate of photoabsorption by calculating both rates at all times during the pulse. The characteristic time scale for energy relaxation in a plasma is controlled by the time taken for an electron at the plasma temperature to undergo a large-angle deflection as the result of scatterings with other electrons in the plasma. Eliezer [34] gives this characteristic time as
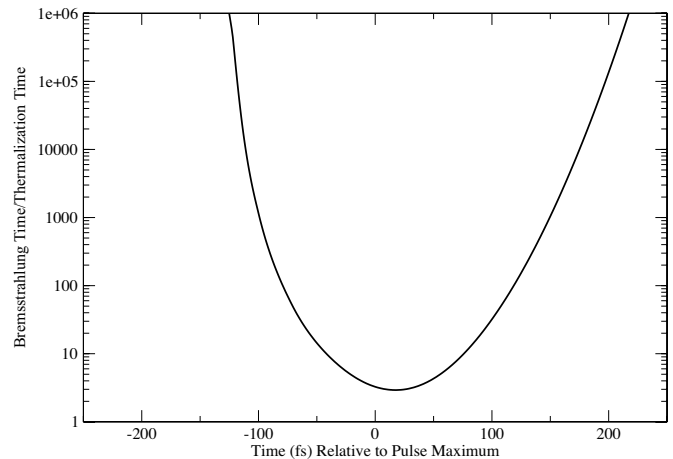

FIG. 5. Ratio of time to undergo stimulated or inverse bremsstrahlung to thermalization time for an electron in the cluster plasma, calculated for a 1500-atom cluster exposed to a 7 $\times 10^{13}$ W/cm^2, 100 fs pulse, using the Wigner-Seitz cutoff model for screening. The electrons thermalize much faster than the bremsstrahlung time throughout the laser pulse.

$$\tau = \frac{3\sqrt{6}}{8} \frac{T^{3/2}}{\pi n_e \ln \Lambda}. \tag{32}$$

We compared this thermalization time to the characteristic time for interaction with the laser beam, defined as the inverse of the total rate of stimulated plus inverse bremsstrahlung processes per electron in the plasma. The resulting ratio, shown in Fig. 5, is highest when the photon flux is low, and falls to a minimum of about 10 when the laser pulse reaches its maximum. We thus find that the plasma electrons reequilibrate much faster than they interact with the laser at all times during the cluster evolution.

For the evolution of the cluster during the period of the laser pulse, we employed a simple model [35] of the cluster expansion that tracks only the radius of the cluster, the evaporation of electrons away from the cluster, and the loss of heat from the electron gas accompanying both processes. We did not consider the possibility of either gross movement of electrons or spatial inhomogeneity of charge species within the cluster, processes that a recent theoretical study [36] has suggested may account for the formation of highly charged ions detected at the Hamburg experiment.

Since all processes considered in our model are at most linear with respect to ion concentration and are integrated over a cluster of finite volume, such quantities as the total rate of energy absorption or the total rates of Xe^{n+} ionizing to form $Xe^{(n+1)+}$ and recombining to form $Xe^{(n-1)+}$ are proportional to the number of ions of the given charge-state found in the cluster, but do not change in the event that the charge-state distribution is inhomogeneous. (This would of course change if we considered an inhomogeneous distribution of electrons, a possibility that is beyond the scope of this paper.) Thus, at the level of approximation used, our model would give identical results if we allowed for spatial inhomogeneity of the various charge species.

The equation for the radius of the cluster is given by

$$\frac{\partial^2 r}{\partial t^2} = 3 \frac{P_e + P_{\text{Coul}}}{n_{\text{Xe}} m_{\text{Xe}}} \frac{1}{r}, \tag{33}$$

where $P_e = n_e T_e$ is the electron pressure and $P_{\text{Coul}} = Q^2/(8\pi r^4)$ is the Coulomb pressure resulting from the charge built up as electrons evaporate away from the cluster.

This model of the laser-cluster dynamics also distinguishes between inner and outer ionization. Inner ionization, which takes place due to photoionization and collisional ionization, is the process by which electrons become liberated from their parent ion and join the cluster plasma, where they can undergo inverse bremsstrahlung heating or collisional ionization or recombination. Outer ionization is the process by which electrons with sufficient energy escape the cluster and cease to have interactions with it.

The rate of evaporation from a Maxwell distribution of electrons can be calculated knowing the size of the cluster, the mean free path of electrons in the cluster, and the temperature of the electron plasma. The rate at which electrons escape from the cluster is then given by

$$W_{fs} = \int_{v_{\text{esc}}}^{\infty} dv \frac{\pi}{4} \frac{\lambda_e}{r} (12r^2 - \lambda_e^2) v f(v), \tag{34}$$

where $v_{\text{esc}} = \sqrt{2(Q+1)/r}$ is the velocity required for an electron to escape from a cluster of charge Q,

$$f(v) = 4\pi n_e (2\pi T)^{-3/2} v^2 e^{-v^2/2T}$$

is the Maxwell distribution, and λ_e is the mean free path in the cluster plasma, given by

$$\lambda_e = \frac{T^2}{4\pi n_e (Z+1) \ln \Lambda}$$

for a plasma with average ion charge Z. The Coulomb logarithm, $\ln \Lambda$, is set equal to the logarithm of the screening length in our calculation of the mean free path. λ_e is constrained to be no greater than $2r$, the diameter of the sphere.

As electrons evaporate from the cluster, the remaining cluster becomes ever more highly charged, and a correspondingly lower fraction of the Maxwell distribution has enough energy to escape the cluster, thereby choking off the evaporation rate.

It is likely that nearly all high-energy electrons detected in the experiment escape during this original period of evaporation. As the cluster expands, the temperature of the electron plasma falls very quickly as electron thermal energy is converted into ion kinetic energy, while the energy required to escape the cluster falls only as $1/r$.

A recent experiment [37] has for the first time measured the energy spectrum for electrons emitted from rare gas clusters exposed to intense vuv light. They give ejection spectra for 70-atom xenon clusters exposed to a 4.4×10^{12} W/cm^2 pulse of vuv light at the same photon energy as the original Hamburg experiment, finding an electron distribution that decreases approximately exponentially according to $I = I_0 \exp(-E_{\text{kin}}/E_0)$, with $E_0 = 8.9$ eV.

We calculated a spectrum of ejected electrons by stepping through a laser pulse using small time steps. For each time step, we calculated the electron density, mean free path, clus-
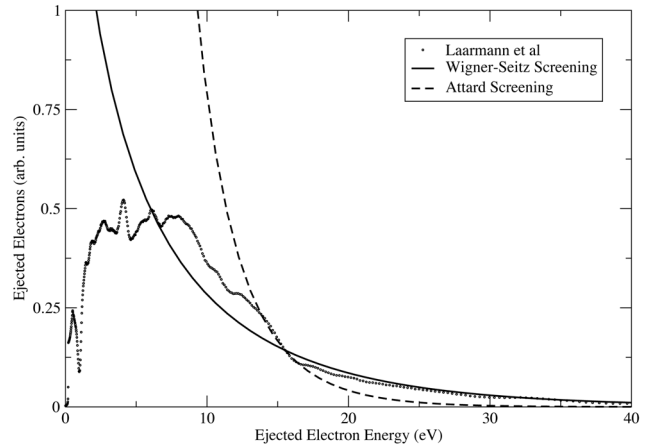

FIG. 6. Ejected electron spectrum. Comparison between data from [37] and spatially averaged spectra calculated using 70-atom clusters exposed to a 4.4×10^{12} W/cm^2, 100 fs pulse for two different models of plasma screening. The Wigner-Seitz cutoff model uses the ordinary Debye length as the screening radius, but the screening radius is not allowed to fall below xenon's Wigner-Seitz radius at liquid density, 4.64 bohr. The Attard model of screening calculates the screening radius according to Eq. (35), discussed in Sec. VI. The spectrum calculated using xenon's Wigner-Seitz radius as a minimum screening distance displays a strong similarity to the experimental curve. The intensity of the experimental spectra is arbitrary; magnitudes were chosen by setting each curve equal at the beginning of the exponential tail in the experiment.

ter radius, and plasma temperature. Using these parameters, we calculated the rate at which electrons with energy $E = E_{\text{esc}} + E_{\text{kin}}$ escaped from the cluster using Eq. (34). Integrated through the time scale of a pulse until the evaporation has stopped, this yields an ejected electron spectrum for a single cluster exposed to the pulse. Since the clusters are located randomly with respect to the center of the laser pulse, we further performed a spatial integration over the radial dimension of the pulse, assuming a Gaussian laser profile $I(r) \propto e^{-r^2/\sigma^2}$ from 0 to 3 σ. The length of the interaction region in the Hamburg experiment was comparable to the Rayleigh range for the laser; accordingly, we assumed a constant laser intensity along the direction of propagation. After performing the spatial integration, we found that on average 0.22 electrons per xenon atom evaporated from the cluster in this way. The spectrum of ejection energies for these electrons shown in Fig. 6, although not exponential, is nevertheless quite similar to the electron spectrum found in Ref. [37].

The largest discrepancy between our calculated spectrum and the spectrum from [37] occurs at low ejection energy. In addition, our model of the cluster expansion predicts that the majority of electrons will comprise electron plasmas, which remain bound to the cluster ions and become quite cold during the process of expansion. These electrons—the great bulk of the population—would reach the detector at low energies and after long delay times, further boosting the spectrum at low energies. However, Laarmann *et al.* note that for $E_{\text{kin}} < 2.5$ eV, coinciding with the region of largest discrepancy, the spectrum cannot be evaluated due to large levels of noise in the background spectra.
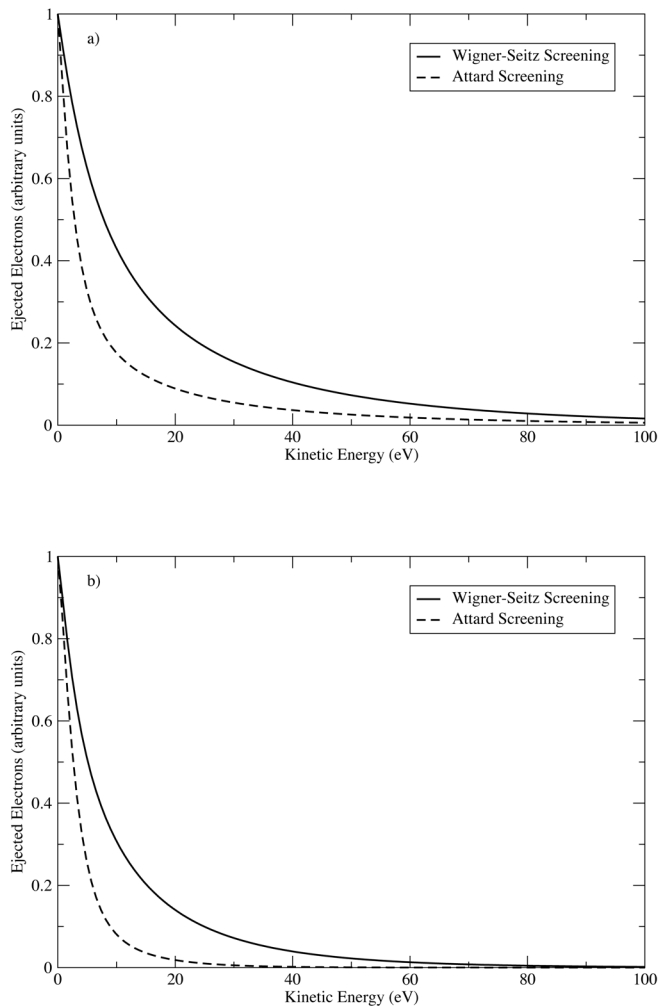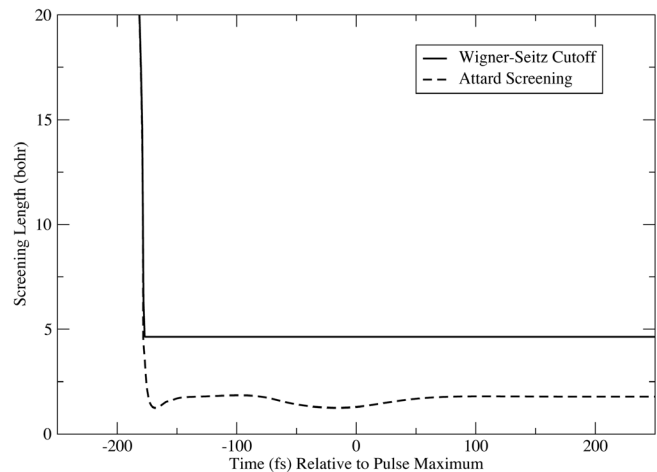
FIG. 8. The description of plasma screening of an atomic potential is unclear as the screening length becomes very short. Here the screening length vs time is given for two simulations of a 1500-atom cluster exposed to a 100 fs, 7×10^{13} W/cm^2 pulse, using two models for screening. In the first model, the screening length is not allowed to fall below xenon's Wigner-Seitz radius at liquid density. The second model for screening uses a formula given by Attard.

FIG. 7. (Color online) Ejected electron spectra, calculated for the two sets of parameters and the two models of screening. The Wigner-Seitz cutoff model uses the ordinary Debye length as the screening radius, but the screening radius is not allowed to fall below xenon's Wigner-Seitz radius at liquid density, 4.64 bohr. The Attard model of screening calculates the screening radius according to Eq. (35), discussed in Sec. VI. (a) Nature parameters: 1500-atom clusters exposed to a 100 fs, 7×10^{13} W/cm^2 pulse. (b) Thesis parameters: 2500-atom clusters exposed to a 50 fs, 2.5×10^{13} W/cm^2 pulse. Since electrons faster than about 1 eV are ejected from the cluster during the pulse, the ejection spectra could serve as a window into the dynamics of the laser-cluster interaction.

Since electrons faster than about 1 eV are ejected from the cluster during the pulse rather than during the slower process of cluster expansion, the ejected electron spectrum has the potential to serve as a window into the nature of the laser-cluster interaction. Accordingly, we give the spectra for 1500-atom clusters exposed to a 100 fs, 7×10^{13} W/cm^2 pulse, and for 2500-atom clusters exposed to a 50 fs, 2.5×10^{13} W/cm^2 pulse in Fig. 7.

After spatial averaging, we find that 1500-atom clusters exposed to a 100 fs, 7×10^{13} W/cm^2 pulse eject 0.22 electrons per atom during this early evaporation period using the Wigner-Seitz cutoff model for the screening length (see Sec. VI for a discussion of plasma screening). Using the Attard

model, 0.07 electrons per atom are evaporated during this period. For 2500-atom clusters exposed to a 50 fs, 2.5×10^{13} W/cm^2 pulse, the corresponding numbers are 0.13 electrons per atom for the Wigner-Seitz cutoff model and 0.02 electrons per atom for the Attard model. In contrast to this, the Hamburg experiment measured an average charge per ion of 2.98. Hence, the electrons that comprise these ejected electron spectra correspond to only a few percent of all free electrons at the time when the expanding clusters reach the detector.

VI. NONIDEAL PLASMA SCREENING

As shown in Fig. 8, when plasma screening of the Xe ions becomes strong enough to allow photoionization of Xe$^+$ into Xe^{2+}, large numbers of extremely low-energy electrons are added to the plasma. As a result, the ratio of electron kinetic energy to electrostatic potential energy falls dramatically, the Debye length of the plasma falls abruptly below the Wigner-Seitz radius of xenon, and the plasma enters a regime of strong correlation. In this regime, a number of the assumptions of the Debye-Hückel screening model break down, and the Debye length loses its meaning as a screening distance [38]. If the plasma cools sufficiently, screening lengths can become complex, and result in oscillatory electron-ion correlation functions [39,40].

Another possibly important effect of the strongly coupled plasma was identified in a recent study [41], which has identified electron dynamics in a strongly coupled plasma as having a very large impact upon rates of many-body recombination and hence upon energy absorption by the cluster as the recombined ions undergo multiple episodes of photoionization.

Most calculations performed in this paper were performed using xenon's Wigner-Seitz radius at liquid density as a

minimum value below which the screening was not allowed to fall. Clearly, with the precise nature of screening unknown in the strongly correlated regime, our method of calculating atomic properties based on a Debye-screened atomic potential acquires a corresponding uncertainty. In an attempt to estimate this uncertainty, we have described the evolution of the cluster using different models for the screening length in a highly correlated plasma.

Our simplest approximation applied xenon's Wigner-Seitz radius at liquid density as a minimum value below which the screening was not allowed to fall. A second model, proposed by Attard [40], deals with ions having a nonzero radius. Strictly speaking, the Debye-Hückel model for plasma screening is invalid except in the limit of ions that have zero size. Attard has shown that in the case in which ions have a nonzero hard-sphere radius d, the screening length $\lambda = 1/\kappa$ differs from the classical Debye-Hückel length $\lambda_D = 1/\kappa_D$ according to

$$\kappa = \frac{\kappa_D}{\sqrt{1 - (\kappa_D d)^2/2 + (\kappa_D d)^3/6}}. \quad (35)$$

This effect becomes important in the domain where $\lambda_D \lesssim d$.

Qualitatively, the effect of considering screening lengths in this model that are shorter than the Wigner-Seitz radius is twofold. First, the tighter screening slightly decreases inverse bremsstrahlung heating. Secondly, it allows photoionization of Xe^{3+} and higher charge states. Directly substituting the Attard screening length for the Debye length with the Wigner-Seitz cutoff, therefore, gives some insight into how sensitive our results are to different models of the ionic potential under very strong screening. As can be seen in Fig. 9, the Attard screening model has a relatively small impact on our prediction for the energy absorbed by the cluster. More prominent is the formation of higher charge states, which is abetted by the reduced ionization potentials resulting from the tighter screening in the Attard model. Figure 10 shows the plasma coupling parameter, a measure for the nonideality of a plasma, for the two models, demonstrating that the Attard screening model gives rise to a more strongly coupled plasma than the pure Debye model. In addition, the two models give different populations for the various charge states at the end of the pulse; however, the combined effects of the cluster expansion and spatial averaging over the beam profile act to destroy much of this information.

As a further test of our model's sensitivity to plasma screening lengths, we calculated the evolution of the cluster in the limit of weak screening. To do this, we fixed the screening length in the cluster at 100 bohr for the entire duration of the laser pulse. In this limit, ionization potentials are unchanged from their values in the absence of screening, and photoionization beyond Xe^+ is impossible. In this model, formation of states with charge 2 or higher must come entirely from collisional ionization. The results of this constraint can be seen in Fig. 11. Neglecting the effects of plasma screening in this way inhibits the formation of high charge states in the cluster, yielding virtually no Xe^{7+} or Xe^{8+}. After the initial photoionization of neutral xenon, the plasma undergoes a period of slow heating while the laser
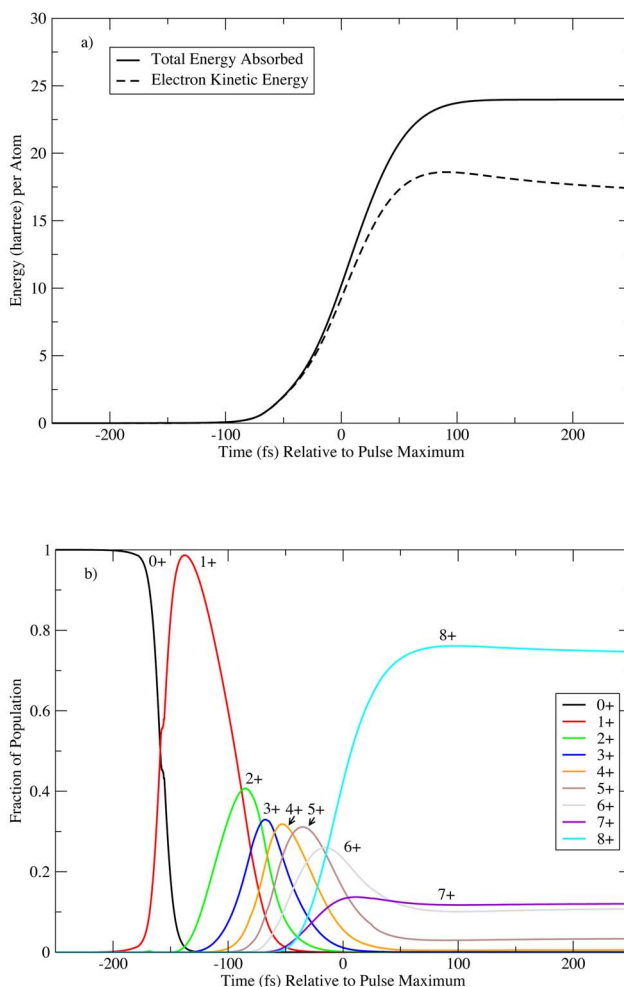

FIG. 9. (Color online) Near the center of the pulse, calculating the evolution of the cluster using Attard screening yields screening lengths shorter than the Wigner-Seitz cutoff, allowing easier formation of high charge states than when the evolution is calculated for Wigner-Seitz screening, shown in Fig. 4. For a 1500-atom cluster exposed to a 7×10^{13} W/cm^2, 100 fs pulse: (a) Energy absorbed vs time for the Attard screening model, (b) charge species population vs time for the Attard screening model.

intensity builds. Near the maximum of the pulse, the plasma becomes energetic enough to ionize the higher charge states with their unscreened ionization potentials, and the rate of inverse bremsstrahlung heating increases rapidly. The total energy absorbed falls from 25 Hartree per atom in the case of the Wigner-Seitz cutoff model to 11.5 Hartree in the limit of no screening.

VII. HYDROGENIC MODEL OF INVERSE BREMSSTRAHLUNG

Most previous approaches to the problem of laser-cluster interactions have considered the ionic potential seen by the electron as a pure Coulomb potential. This is not an unreasonable approximation: as the charge of the ion increases, the difference between inverse bremsstrahlung cross sections calculated using Herman-Skillman potentials and cross sec-
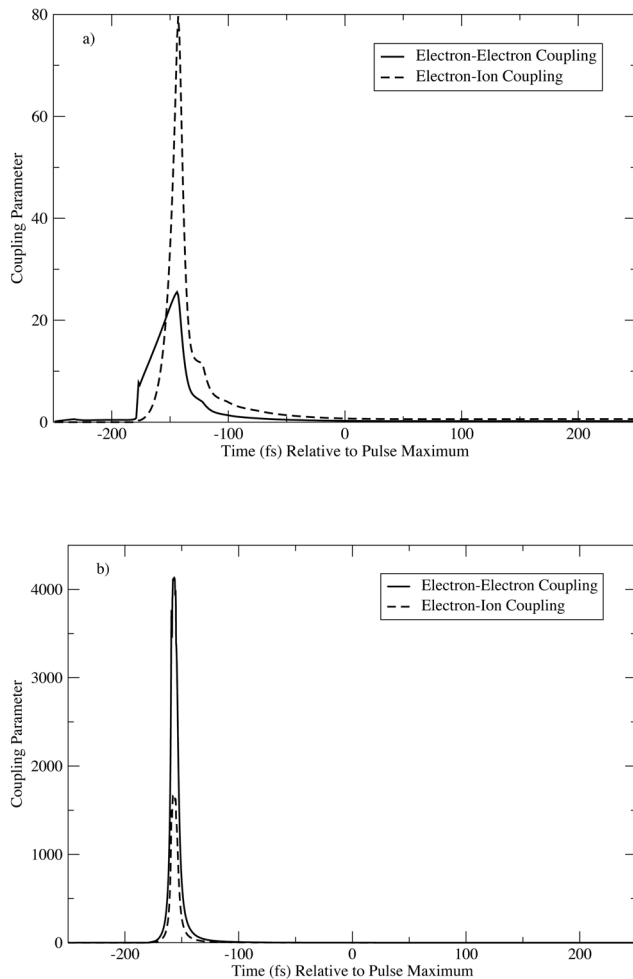
FIG. 10. Plasma coupling parameter vs time for the two models of plasma screening. The coupling parameters are defined by $\Gamma_{ee} = \frac{1}{aT}$ and $\Gamma_{ei} = Z\Gamma_{ee}^{3/2}$, where the average distance between electrons a is given by $a = \left(\frac{3}{4\pi n_e}\right)^{1/3}$ and Z is the average charge of the ions. The plasma becomes very strongly coupled early in the pulse, but the strength of the coupling decreases as the plasma absorbs more energy in the course of the cluster heating. (a) Coupling parameters vs time using Wigner-Seitz cutoff. (b) Coupling parameters vs time for the Attard screening model.

tions calculated using Coulomb potentials is much smaller than in the case of the singly charged ion. This can be seen in Fig. 12, which contrasts inverse bremsstrahlung cross sections calculated using Coulomb and Herman-Skillman potentials for ions of charge 5.

As can be seen in Fig. 4(b), when the laser reaches maximum intensity, most of the cluster has been ionized to such high charge states. Thus, models of the inverse bremsstrahlung process that use Coulombic potentials should be able to see comparable levels of heating to those using cross sections derived using Herman-Skillman potentials.

To investigate this proposition, we simulated the laser-cluster interaction for a 1500-atom cluster exposed to a 100 fs, 7×10^{13} W/cm^2 pulse using our model, but with a physical picture chosen to emulate that of Siedschlag and Rost [36]. In the simulation, we used inverse bremsstrahlung cross sections calculated with Debye-screened Coulomb po-
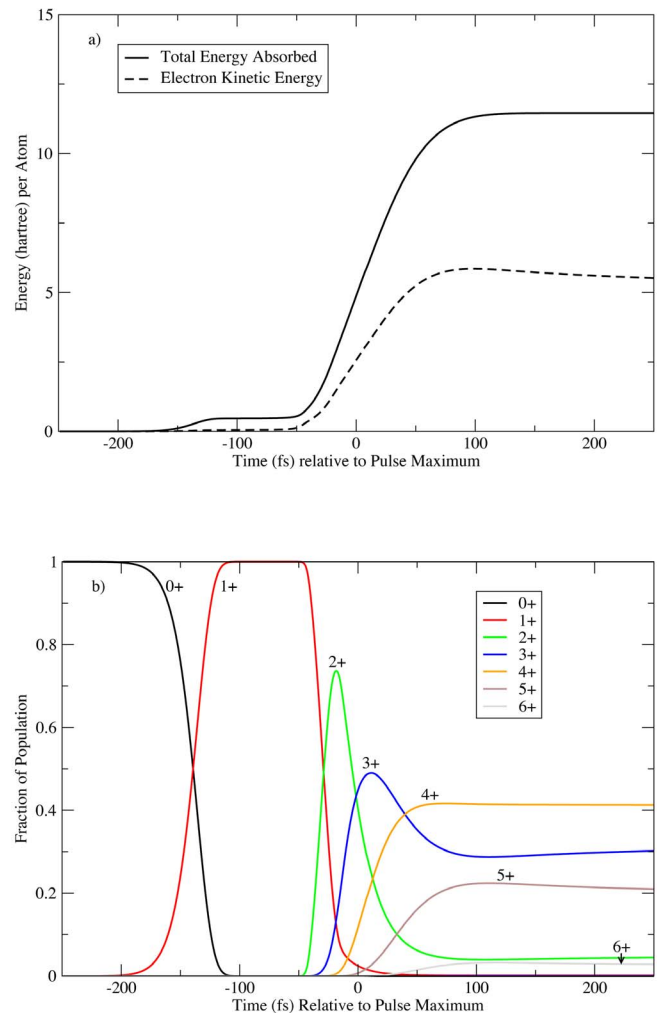

FIG. 11. (Color online) Evolution of the cluster calculated in the limit of long screening length, $\lambda_D = 20$ bohr for a 1500-atom cluster exposed to a 100 fs, 7×10^{13} W/cm^2 pulse. Weak screening prevents ionization potential lowering due to plasma effects, and precludes photoionization past Xe$^+$. The effect of neglecting plasma screening effects is to reduce the formation of high charge states and to reduce the total energy absorbed by the cluster. The pulse and cluster parameters are identical to those used in Figs. 3, 7, and 9. (a) Energy absorbed vs time. (b) Ionic population vs time during laser pulse.

tentials. We used the same ionization potentials and photoionization cross sections as in our other simulations, and used the unaltered Debye length as the screening length. Collisional ionization and recombination were not considered.

The results of this simulation are presented in Fig. 13. We found levels of energy absorption very comparable to those in our own model but very different behavior of the ionic populations with time. Xe^{7+} and Xe^{8+}, which make up almost half of the population of the cluster at the end of the pulse in our model, were present in negligible quantities.

Both differences between the two physical pictures are attributable to the effects of collisional ionization and recombination. Recombination slows the growth of high charge-state populations by allowing some photoionized ions to recombine into a lower charge state, while collisional
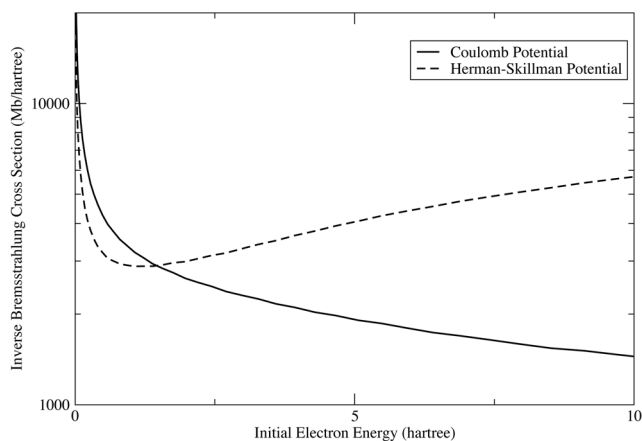
FIG. 12. Inverse bremsstrahlung cross sections [Eqs. (14) and (15)] calculated for an electron in the field of a purely Coulombic 5+ potential and for an electron in the field of a Xe Herman-Skillman atomic potential of the same charge. In comparison with Fig. 1, it can be seen that at higher charge states, the impact of atomic structure on inverse bremsstrahlung cross sections is decreased.

ionization allows the population of charge states that cannot be created via sequential photoionization.

VIII. CONCLUSIONS

When a xenon cluster is irradiated by intense vuv light, there are four phases in its evolution. In the first phase, electrons are liberated from the xenon atoms and form a plasma. As the number of free electrons grows, the screening length of the plasma shrinks.

Once the screening length of the plasma reaches 10.6 bohr, Xe^{1+} can undergo photoionization into Xe^{2+}. This results in the addition of large numbers of low-energy electrons to the plasma, cooling it and decreasing the screening length still further. The ratio of kinetic energy to potential energy falls dramatically, and the plasma temporarily becomes strongly coupled. Ionization potentials for higher charge states fall with increased screening, facilitating their creation.

In the third phase, the plasma undergoes rapid inverse bremsstrahlung heating. High charge states are formed through collisional ionization and recombination, and the cluster becomes charged as energetic electrons evaporate away from its surface. The charge-state distribution shifts rapidly toward higher charges, with the average ionic charge reaching 5.5 at the pulse peak. This distribution changes only slowly on the time scale of the pulse.

Finally, the cluster expands due to the pressure of the electron gas and the cluster's own charge. As the cluster expands, the electron plasma cools and becomes more diffuse. Screening lengths increase, and charge-state equilibrium shifts toward lower charge states.

Of these four phases, our current model describes the first and third phases well, the second more crudely. The dynamics of the expanding cluster are a challenging problem in
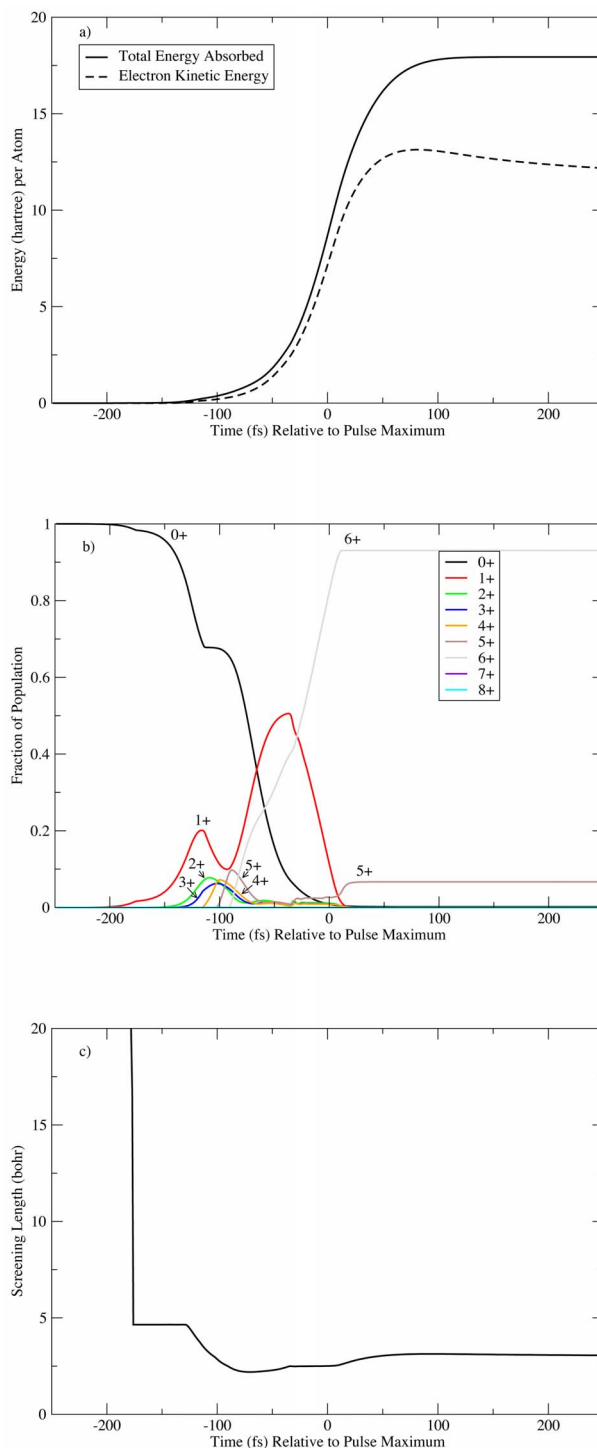

FIG. 13. (Color online) Simulation of the laser-cluster interaction using a physical model taken from [36]. In this model, inverse bremsstrahlung cross sections are calculated using hydrogenic potentials and all high charge states are produced via sequential photoionization. Collisional ionization and recombination are not considered. (a) Energy absorbed vs time. (b) Charge state population vs time. (c) Debye length vs time.

their own right, and demand a treatment more sophisticated than our simple homogeneous expansion model.

For strongly coupled plasmas, it is unclear whether our treatment of plasma screening adequately describes the potential seen by scattering or photoionizing electrons. As the Debye length falls below the Wigner-Seitz radius, the interaction of screening effects due to inner-shell electrons and effects due to screening by continuum plasma electrons should be considered. It is known that the screening length diverges from the Debye length in this limit, but the precise nature of the electron-ion potential is unknown.

There is some difficulty in comparing our results to the Hamburg experiment, due to experimental uncertainty in laser intensity, temporal profile, spatial profile, and cluster size. Whereas in the *Nature* paper the Hamburg group described the laser pulse as 100 fs, 7×10^{13} W/cm^2 incident on 1500-atom xenon clusters, Wabnitz's thesis [42] subsequently describes these pulses as 50 fs, 2.5×10^{13} W/cm^2 pulses incident on 2500-atom clusters. In addition, the temporal profile of the laser pulses is not Gaussian, and varies in an unpredictable way from pulse to pulse due to the nature of the SASE amplification process, which starts from shot noise.

Our model also has difficulty explaining the properties of the clusters long after the laser-cluster interaction is over. As the clusters expand and cool, they continue to undergo collisional ionization and recombination. The distribution of charge states measured at the experimental detectors bears no simple relationship to the distribution we calculate at the end of the pulse. Our homogeneous model of the cluster expansion implicitly requires that all charge states in the same cluster have the same average kinetic energy; this obviously conflicts with the quadratic dependence of energy versus charge state detected in the Hamburg experiment. Also, it is likely that high charge states escape the cluster more quickly than low charge states, spending less time in regions of high electron density and having less opportunity to recombine. Thus, a more sophisticated model of the cluster expansion is necessary in order to predict final charge state and ionic energy distributions with confidence for comparison with experiment.

At the center of a Gaussian laser pulse using parameters taken from the *Nature* paper and a Wigner-Seitz Debye length cutoff, each cluster absorbs on average 682 eV per atom. At a distance of 3σ from the center of such a Gaussian pulse, each cluster absorbs only 0.4 eV per atom. Spatial averaging over the Gaussian pulse profile from 0 to 3σ gives an average of 195 eV per atom absorbed. Using parameters taken from Wabnitz's thesis gives 219 eV per atom at the center, 0.2 eV per atom at 3σ, and 65 eV per atom on spatial averaging.

Using a time-of-flight detector that could detect only charged ions, Wabnitz *et al.* reported an average ion energy of 400 eV, subsequently revised to 650 eV.

Clearly, a spatial average such as we perform could be altered by averaging over a different beam profile or by changing the limits of the radial average and including more clusters that are exposed to only a tiny fraction of the beam's peak intensity. It is also clear that most of the atoms in the clusters that are exposed to very small fractions of the peak intensity will never be ionized and thus would not register in a time-of-flight ion detector such as was used in the Hamburg experiment. Thus, in the absence of better information about the beam's spatial and temporal profile and a more comprehensive model of the cluster expansion after the conclusion of the laser pulse, it is impossible to make precise comparisons between our model and the Hamburg results.

Nevertheless, our model of the laser-cluster interaction explains some surprising features of the laser-cluster interaction in the vuv regime quite well. Primary among these is the surprising efficiency by which the clusters absorb photons. Second, we explain the origin of the high charge states observed in the Hamburg experiment. Third, with the same model we have calculated the early electron ejection spectrum measured in [37] and achieved great similarity to experiment, despite cluster size and pulse intensity that differ significantly from those of the original Hamburg experiment. We have shown that such spectra can depend strongly on the model of plasma screening or the precise parameters of the experiment, and can therefore serve as a possible window into the nature of the laser-cluster dynamics during the time period of the pulse.

In conclusion, we have introduced a model of the laser-cluster interaction in the vuv regime that takes into account improved calculations of inverse bremsstrahlung heating, photoionization, collisional ionization, and recombination. The effects of plasma screening on all of these processes are included, and an alternative model of very strong plasma screening has been considered.

[1] R. F. Service, Science **271**, 920 (1996).

[2] S. Sugano and H. Koizumi, *Microcluster Physics* (Springer, Berlin, 1998).

[3] M. H. R. Hutchinson, T. Ditmire, E. Springate, J. W. G. Tisch, Y. L. Shao, M. B. Mason, N. Hay, and J. P. Marangos, Philos. Trans. R. Soc. London, Ser. A **356**, 297 (1998).

[4] T. Ditmire, T. Donnelly, R. W. Falcone, and M. D. Perry, Phys. Rev. Lett. **75**, 3122 (1995).

[5] Y. L. Shao, T. Ditmire, J. W. G. Tisch, E. Springate, J. P. Marangos, and M. H. R. Hutchinson, Phys. Rev. Lett. **77**, 3343 (1996).

[6] M. Lezius, S. Dobosz, D. Normand, and M. Schmidt, Phys. Rev. Lett. **80**, 261 (1998).

[7] T. Ditmire, T. Donnelly, A. M. Rubenchik, R. W. Falcone, and

M. D. Perry, Phys. Rev. A **53**, 3379 (1996).

[8] J. F. Seely and E. G. Harris, Phys. Rev. A **7**, 1064 (1973).

[9] C. Rose-Petruck, K. J. Schafer, K. R. Wilson, and C. P. J. Barty, Phys. Rev. A **55**, 1182 (1997).

[10] I. Last and J. Jortner, Phys. Rev. A **60**, 2215 (1999).

[11] C. Siedschlag and J.-M. Rost, Phys. Rev. Lett. **89**, 173401 (2002).

[12] T. Seideman, M. Y. Ivanov, and P. B. Corkum, Phys. Rev. Lett. **75**, 2819 (1995).

[13] T. Zuo and A. D. Bandrauk, Phys. Rev. A **52**, R2511 (1995).

[14] A. McPherson, B. D. Thompson, A. B. Borisov, K. Boyer, and C. K. Rhodes, Nature (London) **370**, 631 (1994).

[15] J. Andruszkow *et al.*, Phys. Rev. Lett. **85**, 3825 (2000).

[16] V. Ayvazyan *et al.*, Phys. Rev. Lett. **88**, 104802 (2002).

[17] H. Wabnitz *et al.*, Nature (London) **420**, 482 (2002).

[18] H. Wabnitz, A. R. B. de Castro, P. Gürtler, T. Laarmann, W. Laasch, J. Schulz, and T. Möller, Phys. Rev. Lett. **94**, 023001 (2005).

[19] R. Santra and C. H. Greene, Phys. Rev. A **70**, 053401 (2004).

[20] N. H. Burnett and P. B. Corkum, J. Opt. Soc. Am. B **6**, 1195 (1989).

[21] F. Brandi, I. Velchev, W. Hogervorst, and W. Ubachs, Phys. Rev. A **64**, 032505 (2001).

[22] R. Santra and C. H. Greene, Phys. Rev. Lett. **91**, 233401 (2003).

[23] We use the laser parameters published in Ref. [17]. Recent analysis suggests that the pulse duration in the Hamburg experiment was probably closer to 50 fs and that the intensity was not higher than 3×10^{13} W/cm^2. [Thomas Möller (private communication)].

[24] H. Friedrich, *Theoretical Atomic Physics* (Springer Verlag, Berlin, 1991).

[25] M. Rotenberg, *The 3-j and 6-j Symbols* (Technology Press, Cambridge, MA, 1959).

[26] A. R. Edmonds, *Angular Momentum in Quantum Mechanics* (Princeton University Press, Princeton, NJ, 1996).

[27] M. Aymar, C. H. Greene, and E. Luc-Koenig, Rev. Mod. Phys. **68**, 1015 (1996).

[28] F. Herman and S. Skillman, *Atomic Structure Calculations* (Prentice-Hall, Englewood Cliffs, NJ, 1963).

[29] W. L. Kruer, *The Physics of Laser Plasma Interactions* (Westview Press, Boulder, Co, 2003).

[30] In practice, matrix elements involving large values of l were found to converge very quickly to zero. Because of this, the total transition rate from states of energy E to states of energy E', and hence the heating, is unaffected by the existence of a cutoff.

[31] W. H. Press, S. A. Teukolsky, W. T. Vetterling, and B. P. Flannery, *Numerical Recipes in Fortran 77* (Cambridge University Press, Cambridge, England, 2001).

[32] W. Lotz, Z. Phys. **216**, 241 (1968).

[33] Y. B. Zel'dovich and Y. P. Raizer, *Physics of Shock Waves and High-Temperature Hydrodynamic Phenomena* (Academic Press, New York, 1966).

[34] S. Eliezer, *The Interaction of High-Power Lasers with Plasmas* (Institute of Physics Publishing, Bristol, 2002).

[35] T. Ditmire, T. Donnelly, A. M. Rubenchik, R. W. Falcone, and M. D. Perry, Phys. Rev. A **53**, 3379 (1996).

[36] C. Siedschlag and J.-M. Rost, Phys. Rev. Lett. **93**, 043402 (2004).

[37] T. Laarmann, M. Rusek, H. Wabnitz, J. Schulz, A. R. B. de Castro, P. Gürtler, W. Laasch, and T. Möller, Phys. Rev. Lett. **95**, 063402 (2005).

[38] V. E. Fortov and I. T. Iakubov, *The Physics of Non-Ideal Plasma* (World Scientific, Singapore, 2000).

[39] B. P. Lee and M. E. Fisher, Phys. Rev. Lett. **76**, 2906 (1996).

[40] P. Attard, Phys. Rev. E **48**, 3604 (1993).

[41] C. Jungreuthmayer, L. Ramunno, J. Zanghellini, and T. Brabec, J. Phys. B **38**, 3029 (2005).

[42] H. Wabnitz, Ph. D. thesis, Universität Hamburg (2003).